

Figure 2.16: Photograph of the logic module VUPROM used in the trigger system of the fiber detector. The LVDS ports, at left, are divided in 8 individual ports handling 32 channels each, making a total of 256.

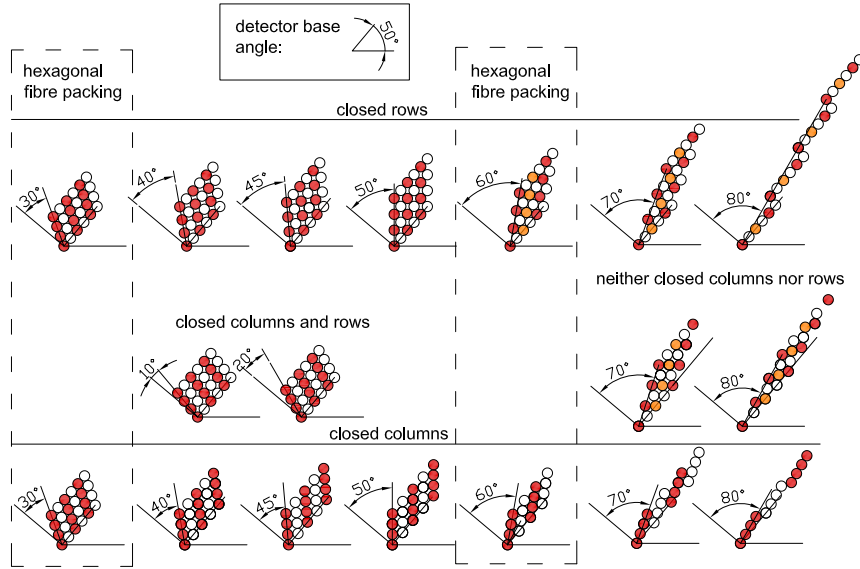


Figure 2.17: Different fiber arrangements geometries with inclined columns. With a ϕ range from 10° to 80° and a rotated detector base of 50° . The upper row shows the geometries with closes row configurations, the lower row, with closed columns. For columns angles of 10° and 20° the configuration is of closed row and columns. Columns angles of 30° and 60° the fiber centers form an hexagonal lattice. For a column angle of 45° the fiber centers are forming a square lattice. Figure from [114].

Nevertheless, in some applications, the incident particle will cross the detection plane with larger angles and would traverse several neighboring columns and compromise the tracking capabilities of such a detector, *e.g.* in the KAOS spectrometer, the average incident angle, w.r.t. a plane following the estimated focal plane at the electron arm, is $\theta = 65^\circ$. The solution is an arrangement with inclined columns w.r.t the detector base. There are many ways to arrange the fiber with inclined columns, however, it has to be able to be built and meet the requirements of the experiments.

Figure 2.17 shows different geometries with different column angles ϕ and four fibers per column. Each geometry corresponds to different arrays with inclined columns. Configurations of closed rows allows larger overlap between neighboring columns, greater spatial resolution and bigger detection efficiency. With columns angles of 30° and 60° , the fibers centers form a hexagonal lattice which provides the highest packing density $\eta_h = \pi/\sqrt{12} \simeq 0.90$, and therefore the most stable structure.

Figure 2.18 (left) shows the ratio of the column pitch to the fiber radius p/ρ , *i.e.* the distance between two neighboring fiber centers, measured perpendicular to the direction of the readout columns. The continuous curve,

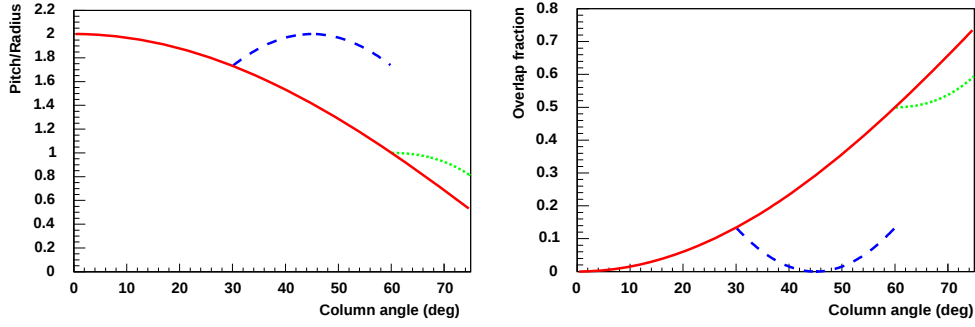


Figure 2.18: The left plot shows the ratio of the column pitch to the fiber radius as a function of the column angle ϕ . The right plot shows the overlap of two neighboring fiber columns in units of the fiber radius. The continuous curve corresponds to a geometry with closed rows, the two branches that are splitting off to geometries with closed columns. Figure from [114].

corresponds to a geometry with closed rows and columns, for which $p/\rho = 2 \cos \phi$. The dashed curve to a geometry with closed columns, where $p/\rho = 4 \sin \phi \cos \phi$ and the dotted curve corresponds a configuration of closed columns with $p/\rho = 4 \sin \phi / \sqrt{9 + \tan^2 \phi}$. In the fiber array for tracking purposes, it is important to avoid gaps between fibers columns losing detection efficiency. Figure 2.18 (right) shows the overlap fraction of two neighboring fiber columns in units of fiber radius o/ρ . It is related directly to the pitch to radius ratio by $o/\rho = (2 - p/\rho)$. Fiber diameter, \varnothing , and overlap fraction are related to the theoretical spatial resolution of the fiber array expected from the geometry. Events in which only one column was hit, the spatial resolution is $\sigma = (\varnothing - 2o)/\sqrt{12}$ and for events in which the particle covered exclusively the inter-column region $\sigma = o/\sqrt{12}$. Averaging both events, $\sigma = \{(\varnothing - 2o)^2 + o^2\}/\sqrt{12}$. For hexagonal packing fiber arrays, the total overlap is $o = \varnothing(1 - 1/\sqrt{2})$ with a pitch of $p = \varnothing/\sqrt{2}$, therefore, the theoretical spatial resolution for such an array is $\sigma = (9/\sqrt{2} - 6)\varnothing/\sqrt{12} \approx 0.1\varnothing$

The energy deposition in a fiber detector is proportional to the detector thickness variation. Figure 2.19 shows the different mass thickness for $\phi = 0^\circ, 45^\circ, 60^\circ$ and 70° . In the hexagonal packing at $\phi = 60^\circ$ the variation is $\delta t \sim 70\% \varnothing$ from minimum to maximum. Although for all other column angles configuration, depending on the geometry, the variation can become smaller, but the difficulty in constructing such geometries make them not viable.

So far in the discussion, only particles crossing the fiber array with the same incident angle as the column angle had been considered. From simulations, the behavior of different arrays for particles crossing the array with different incident angles can be studied. With the use of the Geant4 framework [115], 45° and 60° fiber columns arrangements were simulated with different

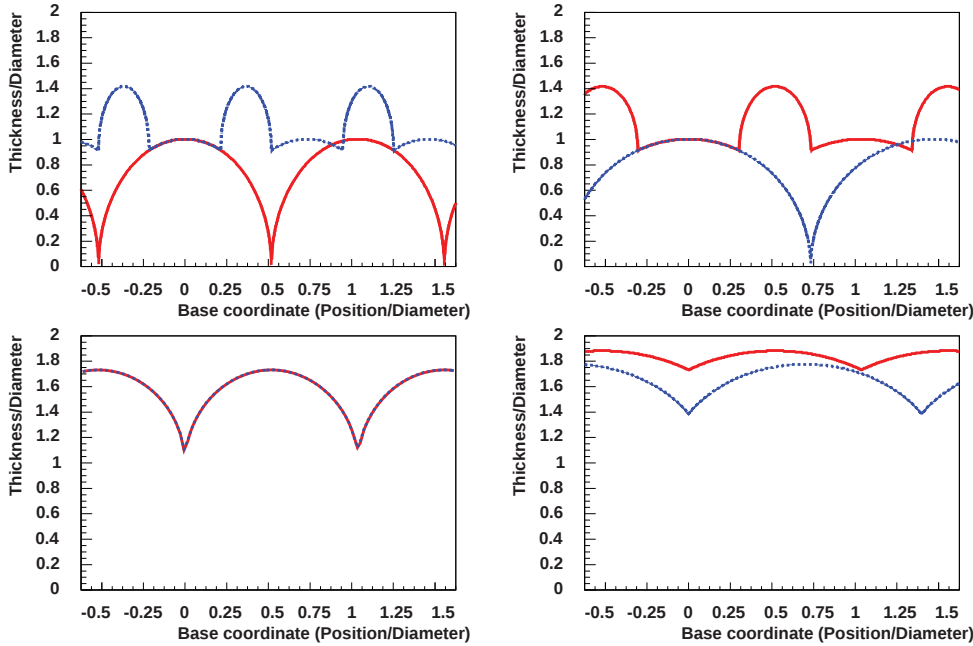


Figure 2.19: Thickness variation as a function of the base coordinate for different fiber array geometries: column angle $\phi = 0^\circ$ (top left), $\phi = 45^\circ$ (top right), $\phi = 60^\circ$ (bottom left), $\phi = 70^\circ$ (bottom right). The two curves correspond to geometries with closed columns (full curve) and closed rows (dotted curve). Figure from [114].

electron incident angles θ with respect to the normal of the detector base. The simulation gave information on the energy deposition in individual fibers and on interactions of the particles with the material as small angle scattering, ionization and bremsstrahlung. The total energy deposited in the active cores of the four corresponding fibers of each column was calculated and signals above a given threshold were assigned to the corresponding read-out channel.

The results from the simulations are presented in fig. 2.20. Multiplicity plots as function of the incident angle show a natural minimum when $\phi = \theta$ and that the multiplicity increases smoothly to a smaller incident angles and steeper to higher angles. It is obvious, from this results, that the columns must be aligned with the direction of the incident's particle and the particle's divergence must be small in order to achieve minimal multiplicity and providing a better spatial resolution.

Simulations can also provide information in order to help to define an optimum threshold where the detector becomes insensitive to particles with larger incident angles θ (fig. 2.20 lower row). The relative thresholds of 100% corresponds to the mean signal of a detector channel for events with incident particles with nominal angle. For incident angles much smaller than the nomi-

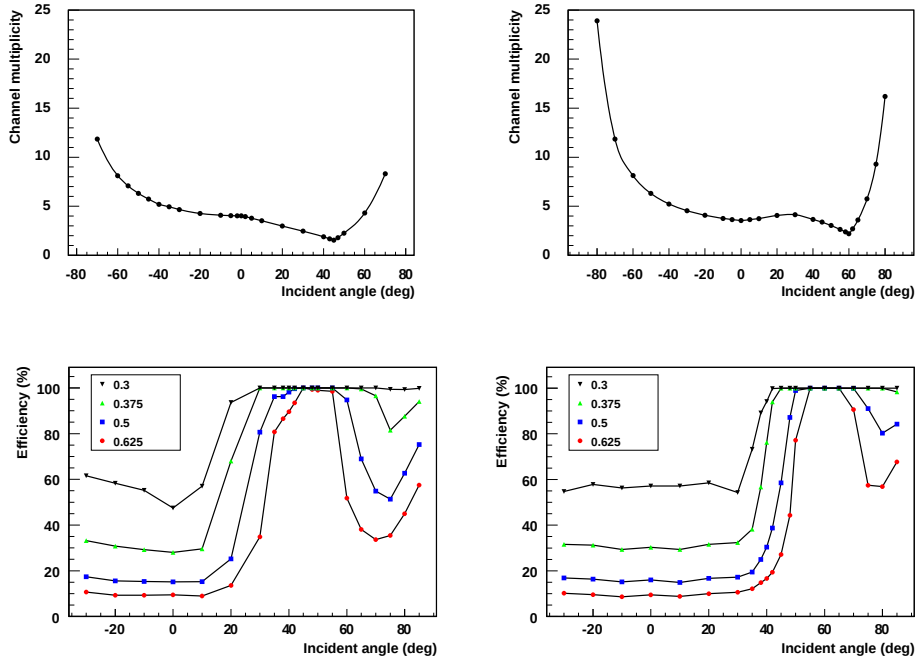


Figure 2.20: (Upper row) Simulated variation of the channel multiplicity as a function of the incident angle θ for fiber array with closed row and columns angles of 45° (left) and 60° . (Lower row) Simulated variation of the efficiency as a function of the incident angle θ for fiber array with closed row and columns angles of 45° (left) and 60° . Figure from [114].

nal angle, only one fiber of each column is hit, but due to the higher multiplicity, many neighboring channels are hit. Therefore, the probability for having a signal in at least one pixel above threshold is strongly dependent on the distribution of energy deposition and the value of the threshold, but independent on geometry and incident angle. [114]

2.4.1.1 Fibers bundles designed in Mainz

The fiber detector concept used in Mainz is based on the fiber hodoscope station in COMPASS [116] therefore the firsts prototypes were based on this design [117]. It consists in 4 double layers with 0.6 mm pitch between two adjacent fibers in the same layer. With this arrangement, the minimum multiplicity is obtained with particles arriving with $\theta = 0^\circ$ w.r.t the normal of the plane generated by the bundle (fig. 2.21). It shows a very stable structure and demonstrates the feasibility of the construction of long fibers arrangements.

Although this design was not suitable for the tracking detector for KAOS spectrometer, it allows an easy way to study the response of the fibers along-

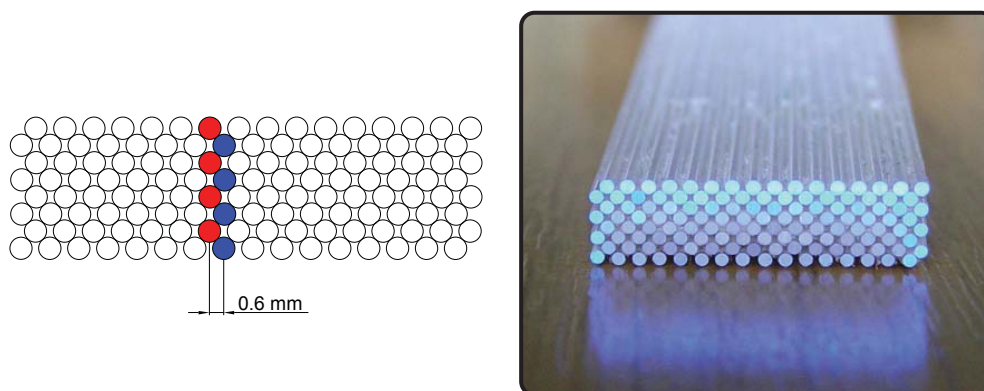


Figure 2.21: Left. Scheme of the fiber arrangement of 0° . Columns of the same color represent a single readout channel. The pitch between each column is of 0.6 mm. Right. Photograph of the bundle arrangement.

side the MaPMT (sec. 3.1).

From this arrangement, a natural slanted columns arrangement can be made with simple translation of the columns. But for symmetry reasons it was adjusted to achieve an inclination of $\phi = 45^\circ$ as shown in fig. 2.22 (left). It has the same pitch between columns of 0.6 mm as the $\phi = 0^\circ$ design. Despite the fact that the design derives from a very stable array, the geometry is intrinsically different and also the construction. Its building process makes it very difficult to obtain a stable array during the gluing phase and many misalignments appear in the final bundle as shown in fig. 2.22 (right). Even some tests were done to study the performance of such an inclined array under beam conditions [118].

As mentioned before, the mean incident angle, estimated from the first simulations, is $\theta \approx 65^\circ$. From the study of the different geometries discussed before, the arrangement closest to the requirements with enough stability is with $\phi = 60^\circ$ with closed row configuration. The pitch between neighboring columns is of 0.42 mm. It has shown a very stable process of construction, giving no deviations of the fiber positions by no more than $0.25\varnothing$. This layout fiber detector was tested in GSI before the serial production of the bundles (sec. 3.2).

2.4.2 Increasing the Light yield

As calculated in sec. 2.1, the light fraction collected in the SCSF-78M multicladding fiber in one side is only of 5.3%. The light directed to the other side is lost if no detector or reflection material is placed. In the KAOS spectrometer, the option of detectors at both sides of the fibers is not possible. Instead, gluing a reflective material, that will decrease the amount of light reflected due to

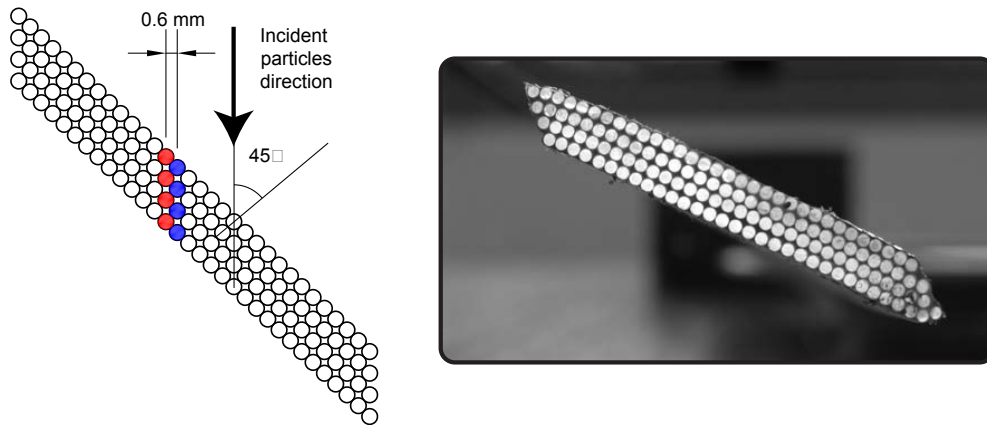


Figure 2.22: Left. Scheme of the fiber arrangement of $\phi = 45^\circ$. Columns of the same color represent a single readout channel. Right. Photograph of the bundle arrangement. The misalignment is visible on the fibers, making it not suitable for tracking purposes.

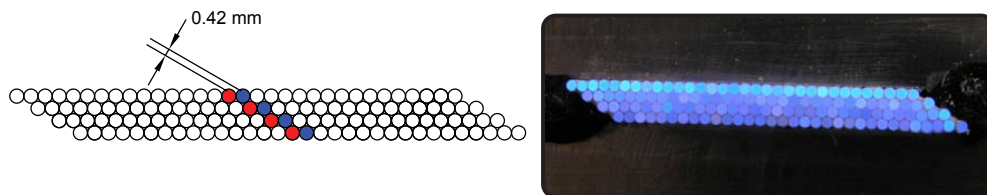


Figure 2.23: Left. Scheme of the fiber arrangement of $\phi = 60^\circ$. Columns of the same color represent a single readout channel. Right. Photograph of the bundle arrangement.

imperfections in the interface fiber-glue-material, some reflective material was vaporized.

It was done through a vacuum chamber with a high current electrode with a tungsten boat where the material pellet to be vaporized is placed. Regular materials for reflection purposes are aluminium or silver. From fig. 2.24 the reflectance at 450 nm, which is the maximum emission of the SCSF-78M (fig. 2.3), is lightly higher for aluminium, $\approx 91\%$ and $\approx 89\%$ for silver. This makes the aluminium an optimum and inexpensive solution.

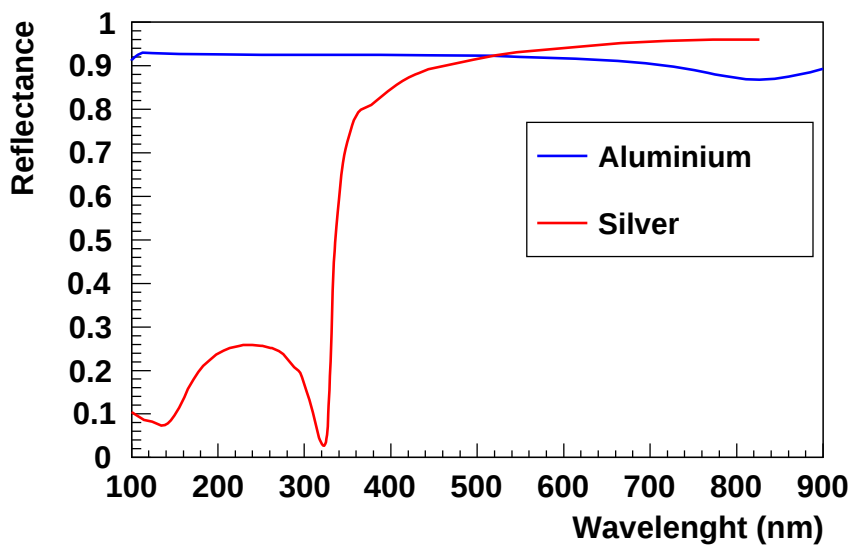


Figure 2.24: Reflectance spectra of aluminium and silver at normal incidence in function of wavelength. Data extracted from [119]

The vacuum chamber (fig. 2.25) consists in a Duran glass cylinder from SCHOTT AG, of 505 mm tall and 335 mm diameter, in a table with a vacuum system and a electrical oven system attached. The vacuum system consists in an air pump compressor, for pre-vacuum, and a jet pump, for high vacuum. On the top of the glass cylinder is an aluminium cap which has a manometer and a pirani for pressure control and also where the fiber bundles are fastened through an extension due to the length of the fibers. The electrical oven is a pair of titanium electrodes holding a tungsten boat with both electrodes connected to a high current supply and covered with a shutter. The system is able to vaporize three bundles at time.

A test with the prototypes of $\phi = 0^\circ$ were done, measuring the ADC of one channel before and after the vaporization. The test with the prototypes

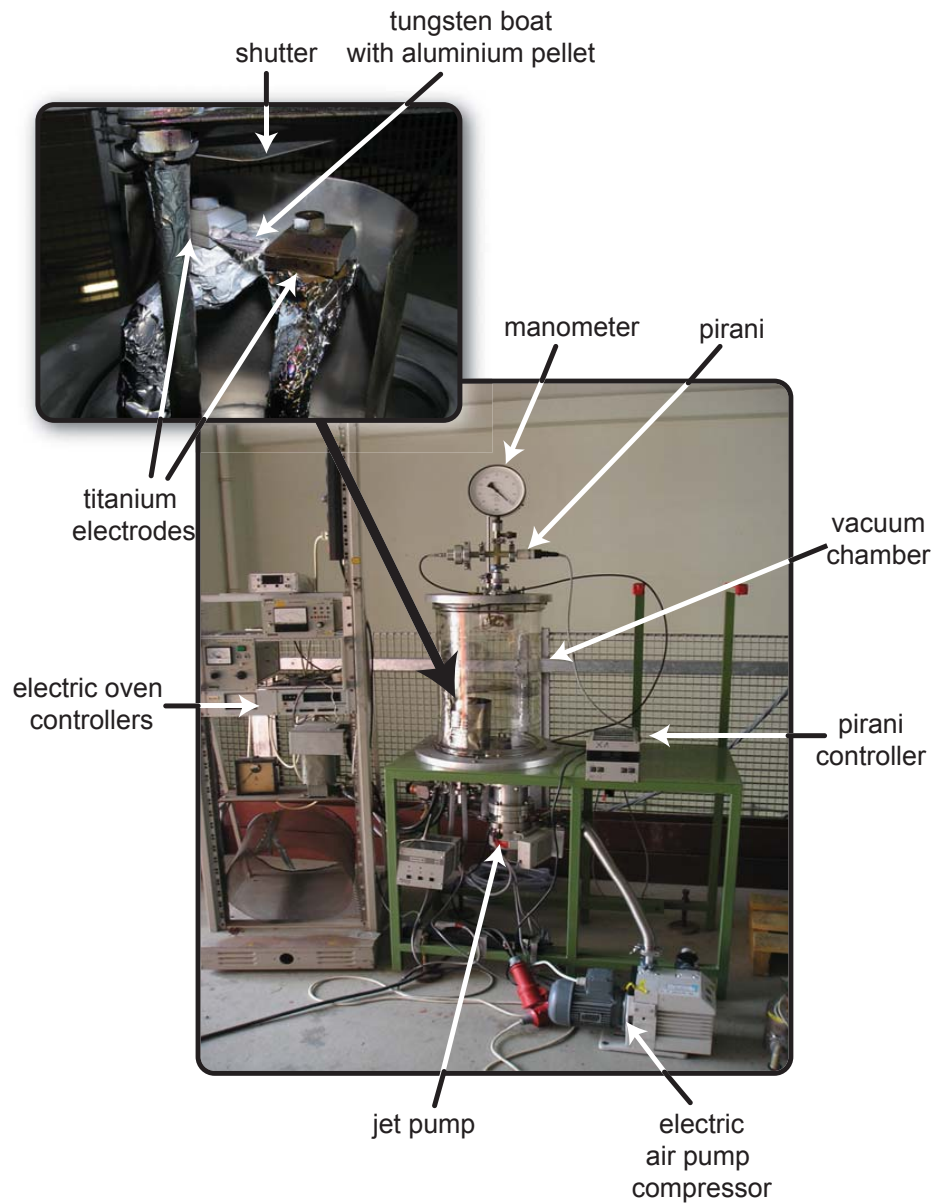


Figure 2.25: Photograph of the vacuum system for vaporization showing the relevant parts of the system. Top left. Detail of the titanium electrodes with an aluminium pellet in the tungsten boat